

Impedance characterization of Quantum Dot

Sensitized Solar Cells

Iván Mora-Seró^{1,*} and Juan Bisquert¹

¹ Grup de Dispositius Fotovoltaics i Optoelectrònics, Departament de Física, Universitat Jaume I, 12071 Castelló, Spain.

*Corresponding Author: sero@uji.es

The development of any technology needs of different characterization techniques that provide an understanding and control of the different processes that constitute that technology. The choice of appropriate characterization techniques for photovoltaic devices can boost the optimization process and determine the effect of the changes performed during this process. In this sense, impedance spectroscopy (IS) has been demonstrated as an excellent technique for the characterization of different kind of photovoltaic devices as Si solar cells,^{1, 2} CdTe thin solid films,³ or dye sensitized solar cells (DSCs).⁴⁻⁶ In this chapter we discuss the use of IS for the characterization of semiconductor sensitized solar cells (SSCs). When the sensitizing semiconductor exhibits quantum confinement these kind of cells are commonly called quantum dot sensitized solar cells (QDSCs).

QDSCs are at first glance structurally similar to DSCs, see Fig. 1, but they use semiconductor materials as light sensitizers instead of the organic or metalorganic dye molecules. However, a more refined study of QDSCs highlights the significant differences with DSCs.⁷⁻¹³ The use of inorganic light absorbers produces a different behavior, that can be analyzed, in some cases, by IS.¹⁴⁻¹⁸ sensitized solar. QDSC are composed by several parts: the wide bandgap nanostructured semiconductor (i.e. TiO₂, ZnO, Sn₂O) that acts as electron transporting material (ETM), the semiconductor sensitizer, the hole transporting media (HTM), commonly a liquid electrolyte, the counter electrode and external contacts and wires, see Fig. 1. IS is a very powerful method that allows to analyze separately each part of the device. IS data can be fitted employing an equivalent circuit. This process permits to obtain important cell parameters provided that a physical model relating the equivalent circuit and the physical properties of each part of the device is employed. In the case of sensitized solar cells, using liquid electrolyte as HTM, the model employed for analyze the IS results is displayed in Fig. 1.^{5, 15, 19} The elements of the equivalent circuit are related with the physical processes occurring in the device.

- C_{μ} ($=c_{\mu}/L$, where L is the TiO₂ layer thickness) is the *chemical capacitance* that stands for the change of electron density as a function of the Fermi level, and it monitor the distribution of traps states in the bandgap of the TiO₂ semiconductor. Chemical capacitance provides valuable information on the TiO₂ conduction band (CB) position.
- R_{tr} ($=r_{tr}\cdot L$) is the *electron transport resistance* in the TiO₂, directly related to the reciprocal of electron conductivity in TiO₂, σ_n :

$$\sigma_n = L / R_{tr} \cdot S \quad (1)$$

where S the geometry area.

- R_{rec} ($=r_{rec} \cdot L$) is the *recombination resistance*, a charge-transfer resistance at the TiO_2 /sensitizer/electrolyte interface related to recombination of electrons in the TiO_2 with acceptor species in the electrolyte and/or sensitizer. R_{rec} is inversely proportional to the recombination rate and the density of electrons in TiO_2 .
- R_s is a series resistance accounting for the transport resistance of the transparent conducting oxide and the connection setup. Z_d is the diffusion impedance of the redox species in the electrolyte.
- R_{ce} represents the charge transfer resistance at the counter electrode/electrolyte interface. C_{ce} is the interfacial capacitance at the counter electrode/electrolyte interface.

The first three mentioned elements (C_μ , R_{tr} and R_r) are denoted in lowercase letters in Figure 2c meaning the element per unit length for a film of thickness L , because they are distributed in a repetitive arrangement of a transmission line. The physical meaning of this network corresponds to the impedance of diffusion and recombination.⁴ The IS model presented allows an easy correlation between the impedance spectra and the physical processes, permitting to distinguish separately each effect.²⁰ This model can be extrapolated for all-solid devices, with solid HTM, implementing slight modifications to the equivalent circuit in Fig. 1, mainly to take into account the transport along the HTM.²¹⁻²⁴

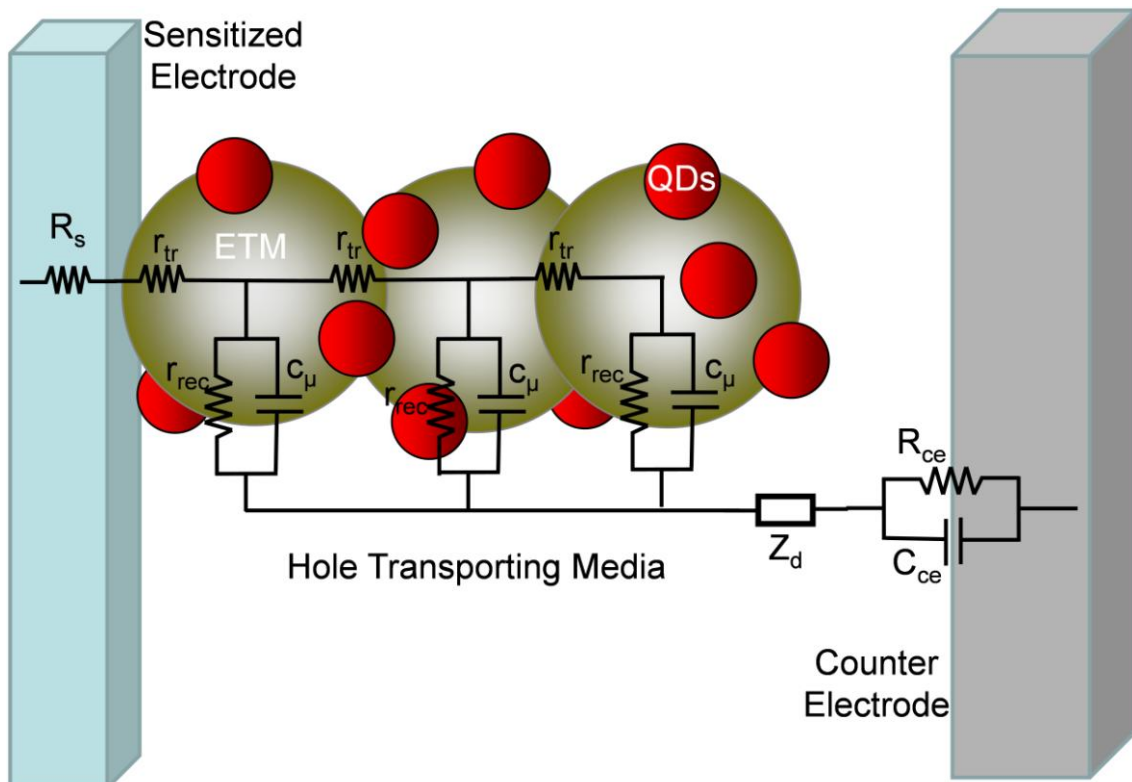


Fig. 1:Equivalent circuit for impedance analysis of QDSCs. Nanostructured electrode of an electron transporting material (ETM) is sensitized with quantum dots (QDs). After electron-hole photogeneration in QDs electrons are transferred to ETM while holes are transferred to hole transporting media (electrolyte or solid hole conductor). Finally holes are collected at the counter electrode. In the cartoon equivalent circuit is plotted on overlapping the cell configuration to give an orientation of the relation between each circuit element and the part of the cell where the related process occurs.

In an impedance measurement a DC bias is fixed and a small AC perturbation is applied at different frequencies. At each frequency the impedance value Z is obtained, and represents a point in the complex plane impedance plot. The points obtained for the different frequencies produce an impedance spectra as the ones represented in Fig. 2, where several examples of complex plane impedance plots for QDSCs are shown. In this plot the imaginary part of impedance (generally changed of sign), $-Z''$, is represented against the real part of impedance Z' , where the impedance is

$$Z = Z' + j Z'' \quad (2)$$

with $j = \sqrt{-1}$. The points obtained at the higher frequencies, where capacitances can be considered short circuits, are the points close to $Z'=0$. As the frequency of the AC signal decreases the obtained points move to higher Z' values.

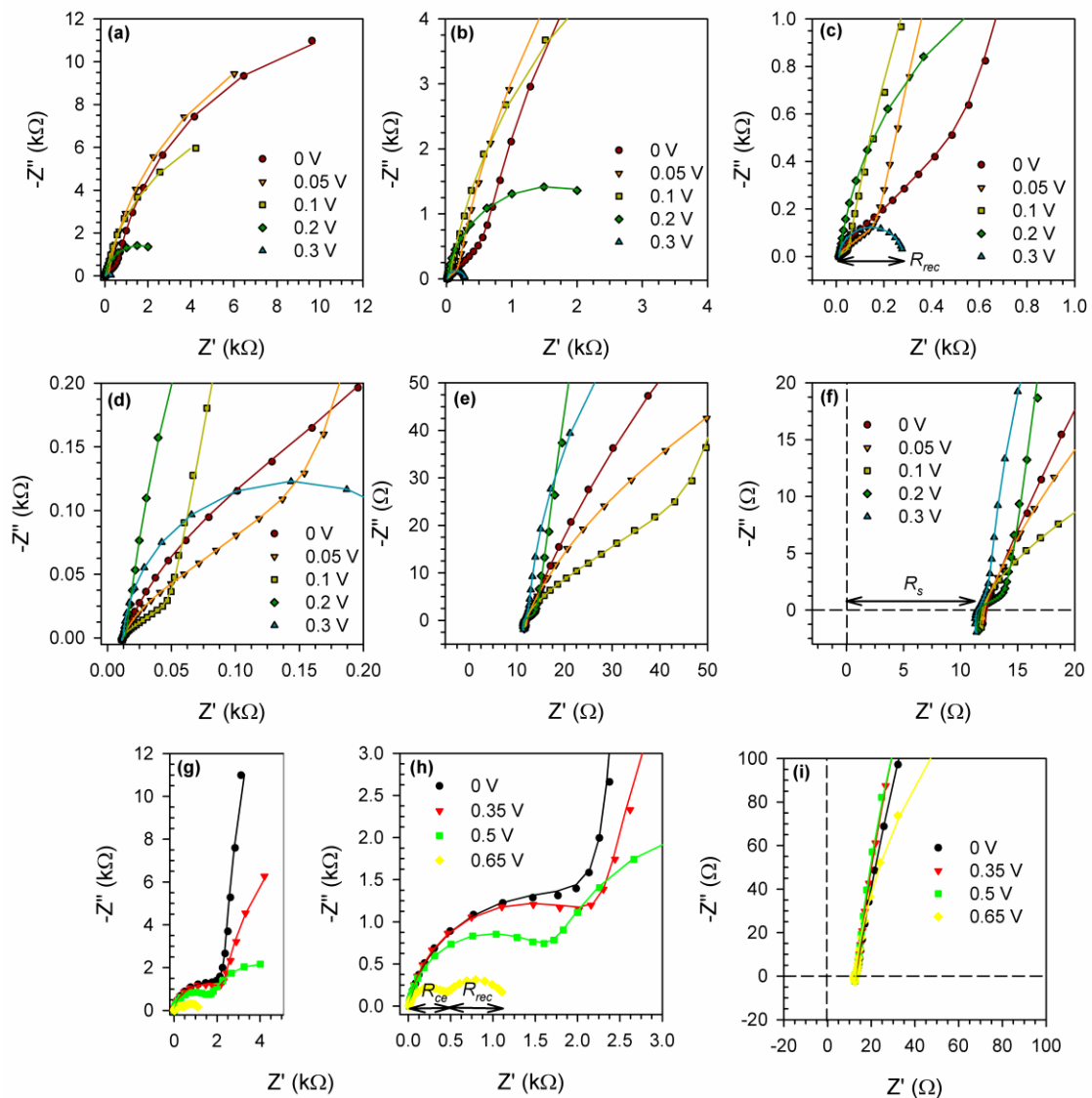


Fig. 2: Complex plane impedance plots of some QDSCs at different applied forward bias (indicated in the legend). (a)-(f) PbS/CdS/ZnS QDSC¹⁴ sensitized by SILAR using 2, 5 and 2 cycles respectively, TiO₂ nanoparticles have been used for nanostructured electrode, polysulfide electrolyte and Cu₂O counter electrode. (b) to (f) are successive zooms of the high frequency region of the precedent graph. (g)-(h) CdS/CdSe/ZnS QDSC²⁵ sensitized with CdS by CBD and with CdSe/ZnS by SILAR using 6 and 2 cycles respectively, TiO₂ electrospun nanofibers have been used for nanostructured electrode, polysulfide

electrolyte and platinized counter electrode. (h) to (i) are successive zooms of the high frequency region of the precedent graph. Solid line are the fitting obtained with the equivalent circuit in Fig. 1.

In the impedance spectra reported in Fig. 2, a frequency range between 1 MHz and 0.1 Hz has been employed. The solid lines are the fittings obtained with the equivalent circuit in Fig. 1, an excellent agreement between experimental point and fitted results are obtained. In Fig. 2(a)-(f) impedance spectra at various applied forward bias are depicted. These spectra corresponds to a PbS/CdS/ZnS QDSC¹⁴ sensitized by Successive Ionic Layer Absorption and Reaction (SILAR)^{26, 27} using 2, 5 and 2 cycles respectively, TiO₂ nanoparticles have been used for nanostructured electrode, with polysulfide electrolyte and Cu₂O counter electrode. In these graphs, Fig. 2(a)-(f), the characteristic pattern of the transmission line, TL, (the circuit constitute for r_{tr} , r_{rec} and c_{μ} in Fig. 1) is clearly observed at low frequencies. The TL pattern is form by a straight line followed by semicircle, and it is observed at low frequencies in Fig. 2(a)-(f). The diameter of the semicircle is R_{rec} , Fig. 2(c) and the parallel association with C_{μ} , produces the apparition of the semicircle.⁴ Note that the diameter of the semicircle decreases as the forward applied bias increases, we will explain this behavior below. Forward bias is defined as a voltage that moves the electron Fermi level in TiO₂ up. For low voltage applied bias we don't see the complete semicircle as measurement points at lower frequencies are needed in this case, but in any case the reported data is enough to fit the spectra in order to obtain R_{rec} and C_{μ} . The coupling between R_{tr} and R_{rec} - C_{μ} produces the straight line before the semicircle, the length of this straight line is related with the R_{tr} value.^{5, 19} From Fig. 2(a)-(f), it can be clearly observed that the R_{tr} value decreases with the applied forward bias as R_{rec} . The straight line becomes too small to be observed at high voltages, consequently R_{tr} cannot be determined when the straight line is not observed.

On the other hand, one very important parameter for solar cell performance is the series resistance, R_{series} , as it affects deleteriously the fill factor, FF, and even the photocurrent if this resistance is large enough.²⁸ There are several contributions to $R_{series} = R_s + R_{ce} + R_d$. R_s , due to wire and contacts, and the total series resistance can be easily determined from the impedance spectra as it is indicated in Fig. 2(f). R_{ce} is the charge transfer resistance at the counter electrode, coupled with the capacitance of electrolyte/counter electrode interface provides an additional semicircle at high frequencies.^{5, 19} R_d is a resistance due to the diffusion in the electrolyte. It can be obtained from a third semicircle at low frequencies. This semicircle is not observed in the spectra plotted in Fig. 2, as it is observed at higher applied voltage and for frequencies lower than the range used in the experiments here provided. Additional examples of this resistance and how determine it from impedance spectra in references 5, 19.

The semicircle at high frequencies due to the parallel association of R_{ce} and C_{ce} . It cannot be fully appreciated in Fig. 2(a)-(f), as it couples with the straight line from the TL, and it can be observed as a humping at high frequencies. This semicircle can be easily appreciated in Fig. 2(g)-(i) as R_{ce} is bigger than in Fig. 2(a)-(f). In fact, the growth of R_{ce} prevents to appreciate the straight line of the TL. In this cases, the equivalent circuit in Fig. 1 can be simplified and the TL (the circuit constitute for r_{tr} , r_{rec} and c_{μ} in Fig. 1) can be replaced for a parallel association of R_{rec} and C_{μ} . Examples of this simplified circuit can be found in references: 16, 18, 25. Thus, R_{ce} and R_{rec} can be obtained from the diameter of the first and second semicircles, see Fig. 2(h). The results plotted in in Fig. 2(g)-(i) corresponds to CdS/CdSe/ZnS QDSC²⁵ sensitized with CdS by Chemical Bath Deposition (CBD) and with CdSe/ZnS by SILAR using 6 and 2 cycles respectively, TiO₂ electrospun nanofibers have been used for nanostructured

electrode, with polysulfide electrolyte and platinized counter electrode. The significantly different values for observed in Fig. 2(a)-(f) in comparison with Fig. 2(g)-(i) will be analyzed below. It is also interesting to comment that an inductive (positive Z'') behavior is observed at the highest frequencies, see Fig. 2(f) and 2(i), due to the wires for connections of the experimental setup. An inductance in series with the equivalent circuit, can be used to fit this part of the impedance spectra.

The definition of an equivalent circuit is only a step in the IS analysis process. Obviously, it is required that each part of the equivalent circuit is related with a physical process, as it is already commented, and verify that this relationship is correct. To perform such analysis, impedance spectra is fitted with the equivalent circuit model at *different* applied voltages, V_{app} , (at different electron Fermi levels).^{5, 19, 29} It is subsequently observed if the obtained behavior correspond to the expected evolution of that parameter in relation with the physical process represented. If the verification is not successful another model has to be proposed and verified again.

When the correct model is obtained, like the one reported in Fig. 1 for DSCs and QDSCs, the IS analysis can provide us abundant and important information about solar cell performance. Hereafter, we are going to show some examples of the different parameters that we can be obtained with the IS characterization, and how this information can help us to understand the solar cell performance.

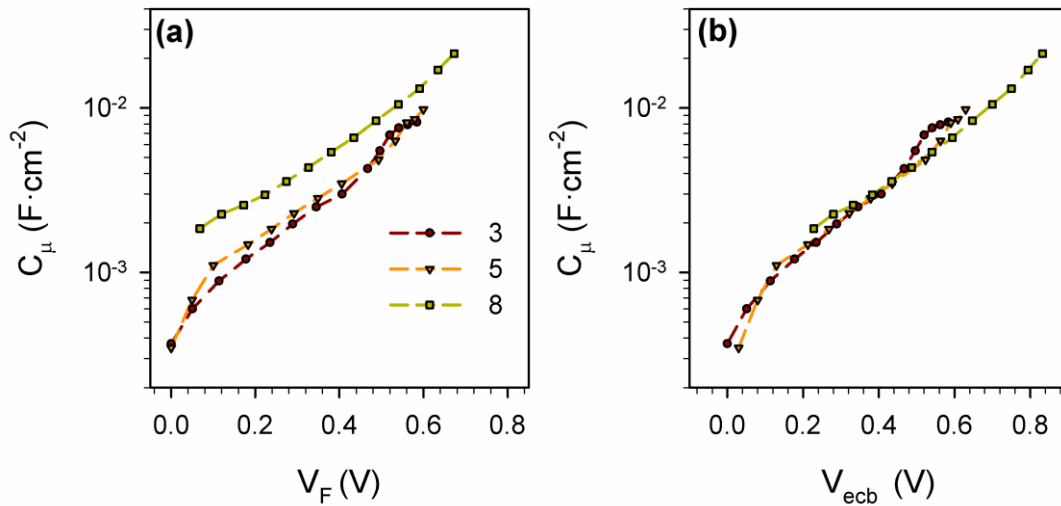


Fig. 3:Chemical capacitance, C_{μ} , of QDSCs represented vs. (a) voltage drop in the sensitized electrode V_F and vs. (b) the equivalent conduction band V_{ecb} . CdSe/ZnS QDSC sensitized by SILAR using different number of CdSe cycles as indicated in the legend and, TiO_2 nanoparticles have been used for nanostructured electrode, polysulfide electrolyte and Cu_2O counter electrode.¹⁵ Reproduced with permission from ACS Nano.

Chemical capacitance for CdSe/ZnS QDSC sensitized by SILAR using different number of SILAR cycles is plotted in Fig. 3, vs. V_F (Fig. 3(a)) and vs. V_{ecb} (Fig. 3(b)). V_F is the voltage drop in the sensitized electrode. This voltage is proportional to the rise of the Fermi levels of electrons in TiO_2 and is obtained removing the effect of the series resistance as $V_F = V_{app} - V_{series}$. i.e. subtracting from V_{app} the potential drop at the series resistance, V_{series} .^{5, 15, 16, 18} The representation against V_F allows a comparison between sensitized electrodes removing the effect of the rest of the solar cell and it is interesting if we want to compare cells with changes only in the sensitized electrode. From Fig. 3(a) it can be observed that the chemical capacitance of nanostructured TiO_2 electrodes,

prepared in the same conditions, is shifted to lower potentials as the number of CdSe SILAR cycles increases. This shift is due to a downwards displacement of the TiO₂ conduction band (CB). The position of TiO₂ CB plays an important role in the final efficiency of sensitized solar cells, as it affects the open circuit potential, V_{oc} , and the short circuit photocurrent, J_{sc} .³⁰ If the recombination process do not vary a downwards movement of TiO₂ CB increase the driving force for electron injection into TiO₂ from dye or QD, enhancing J_{sc} . But reduces the V_{oc} . An upwards displacement of TiO₂ CB produces the opposite effect, always considering no change in the recombination rate. Note that to appreciate the CB shift is important to plot results at different potentials. There are many examples in the literature comparing impedance result at a single potential. In this case the shift of TiO₂ CB cannot be evaluated and consequently the origin observed behavior cannot be unambiguously determined. We strongly suggest an analysis including different applied forward voltages.

When we try to compare two cells with different TiO₂ CB, to explain the observed changes we have the problem of discriminating between the effect of the CB displacement and a modification of the recombination. Recombination rate depend on the electron density in TiO₂ CB, n . Thus, to compare strictly the recombination without the effect of the CB displacement V_F is not a good reference. V_F is proportional to the rise of the Fermi level of electrons in TiO₂, $V_F = (E_{Fn} - E_{F0})/q$, where q is the positive elementary charge and E_{Fn} and E_{F0} are the electron Fermi level and the electron Fermi level at the equilibrium respectively.¹¹ An important tool to correctly evaluate the parameters dependent of TiO₂ CB position is therefore to plot these parameters of different devices at the same equivalent value of the position of the conduction band compare the voltage drop in a “common equivalent conduction band” V_{ecb} . To analyze different cell parameters on the basis of a similar electron density (i.e. the same distance between the electron Fermi level, E_{Fn} , and CB of TiO₂, ΔE_{CB} , the shift of CB has to be removed as in Fig. 3(b), where the voltage scale is $V_{ecb} = V_F - \Delta E_{CB}/q$. The criterion for the modified scale is that the chemical capacitances of all the analyzed samples overlap; see Fig. 3(b), because the chemical capacitance is directly related with the difference $E_{CB} - E_{Fn}$, by the relation $C_{\mu} \propto \exp[-(E_{CB} - E_{Fn})/k_B T]$.³¹ The same shift applied to the chemical capacitance has to be applied to the other parameters in order to compare them vs. V_{ecb} , as in Fig. 4(c).

In Fig. 4 the different resistances obtained for several QDSC, employing the equivalent circuit in Fig. 1. R_s , the series resistance introduced by wires and connections, is compared for cells with different CdSe SILAR cycles in Fig. 4(a). R_s is expected to be independent of the applied voltage and on the number of SILAR cycles as observed in Fig. 4(a) for cells with 5 and 8 SILAR cycles. The increase of R_s observed for the cell with 3 SILAR cycles is not due to the sensitization process of the electrode, but in this case no metallic contact was soldered on transparent conductive electrode. This soldered contact reduces effectively R_s .¹⁵ In Fig. 4(b) QDSCs with polysulfide electrolyte using different counter electrodes are compared. Platinized counter electrode presents a high charge transfer resistance, R_{ce} , with the polysulfide electrolyte, originating an increase of the solar cell series resistance and consequently a decrease in the FF and in the final conversion efficiency.^{15, 16} In QDSCs with platinized counter electrode R_{ce} increases significantly and it is not possible to observe the straight line of the TL, as it is the case in Fig. 2(g)-(i). On the other hand when Cu₂S counter electrode is used the R_{ce} , decreases significantly, see Fig. 4(b), then the size of the first semicircle (at high frequency) in the Nyquist plot is reduced and the straight line of the transmission line can be easily appreciated, see Fig. 2(a)-(f).

Recombination resistance for different cells is compared in Fig. 4(c). To rule out the effect of different TiO_2 CB position R_{rec} is plotted against V_{ecb} , simply by applying to the recombination resistance the same shift that has been applied to C_μ to make all the capacitances overlap, see Fig. 3(b). In the case of Fig. 4(c) we observe an increase of the recombination resistance with the number of SILAR cycles. As recombination rate is inversely proportional to R_{rec} , QDSCs with higher number of CdSe SILAR cycles present lower recombination rate than the cells prepared with lower SILAR cycles. The recombination decrease, when the other parameters are kept unchanged, produce an increase of the V_{oc} .⁵ Thus, for cells with high number of CdSe SILAR cycles a reduction of the V_{oc} should be expected from the downward shift of TiO_2 CB, Fig. 3(a). But this effect is compensated by the lower recombination observed in Fig. 4(c). As a consequence the V_{oc} does not decrease (even increases slightly) with the number of CdSe SILAR cycles.¹⁵ R_{rec} decreases exponentially with voltage as the recombination rate is proportional to n and n increases exponentially with Fermi level (V_F).

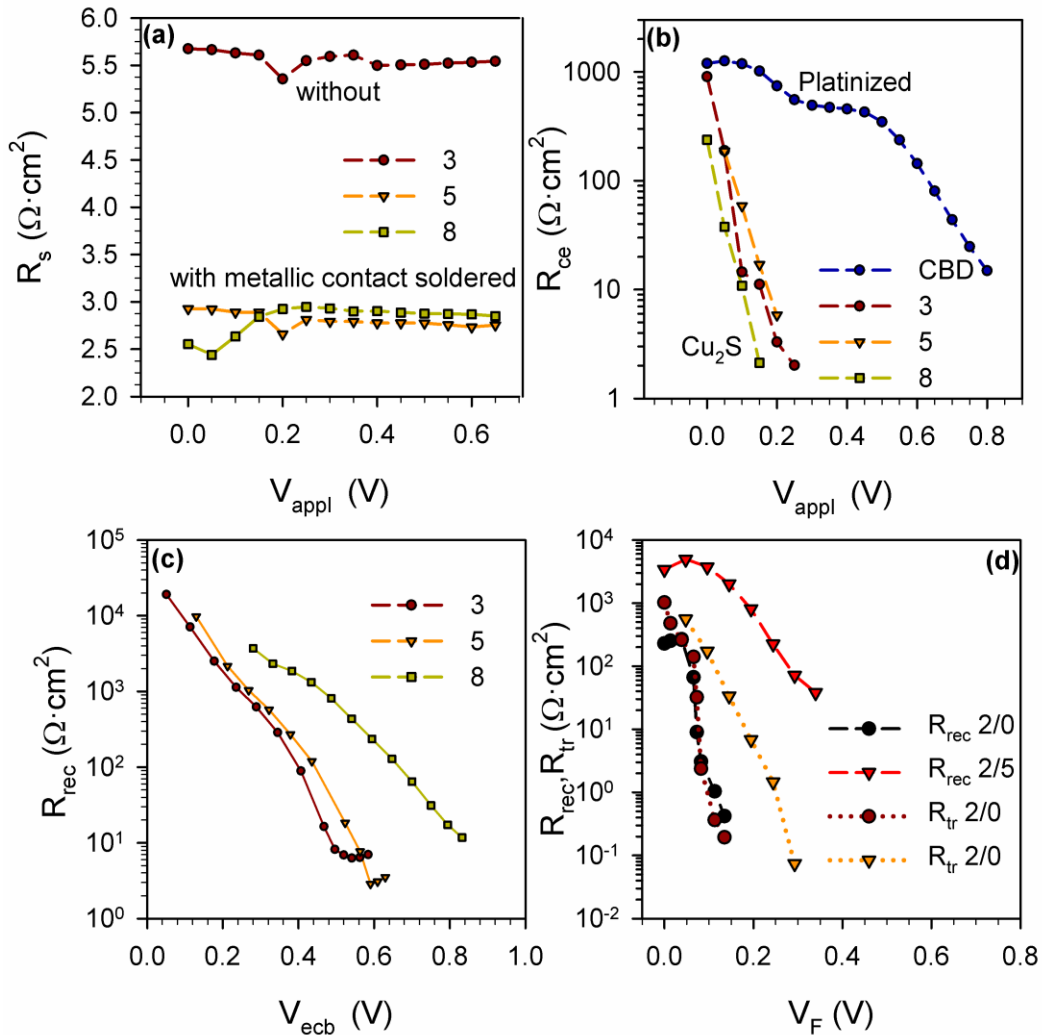


Fig. 4: Resistances of QDSCs. (a) Series resistance, R_s ; (b) transport resistance, R_{tr} , and (c) recombination resistance, R_{rec} , of CdSe/ZnS QDSC sensitized by SILAR using different number of CdSe cycles as indicated in the legend and 2 SILAR cycles of ZnS, TiO_2 nanoparticles have been used for nanostructured electrode, polysulfide electrolyte and Cu_2O counter electrode.¹⁵ Reproduced with the permission of ACS Nano. (d) R_{tr} and R_{rec} of PbS/CdS/ZnS QDSC sensitized by SILAR using different number of PbS/CdS cycles as indicated in the legend and 2 SILAR cycles of ZnS, TiO_2 nanoparticles have been used for nanostructured electrode, polysulfide electrolyte and Cu_2S counter electrode.

nanostructured electrode, polysulfide electrolyte and Cu_2O counter electrode.¹⁴ Reproduced with the permission of Journal of Physical Chemistry Letters.

When the counter electrode is good enough to reduce the charge transfer rate with the electrolyte, the straight line from the TL can be clearly observed, see Fig. 2(a)-(f). In those cases, transport resistance of electrons in TiO_2 can be determined, see Fig. 4(d). For a good cell performance it is needed that $R_{rec} \gg R_{tr}$, in the other case the cell performance is limited by the electron transport.^{4, 5, 19} In Fig. 4(d), we have the two QDSCs with different light absorbing material PbS/ZnS (efficiency $\eta=0.51\%$) and PbS/CdS/ZnS ($\eta=2.21\%$) and significant difference in the cell performance.¹⁴ In Fig. 4(d) it can be observed that, for PbS/CdS/ZnS, the R_{rec} is significantly higher than R_{tr} as correspond to a good performing solar cell. On the other hand, the cell with no CdS protecting PbS presents similar values of R_{rec} and R_{tr} and a poor performance is expected, as it is in fact the case.

In addition to capacitances and resistances related with the physical processes that take place in the solar cell, other interesting parameters for electronic processes in TiO_2 can be derived from the previous ones, as the conductivity, eq. 1 and Fig. 5(a), electron lifetime, Fig. 5(b), diffusion coefficient, Fig. 5(c), and diffusion length, Fig. 5(d)

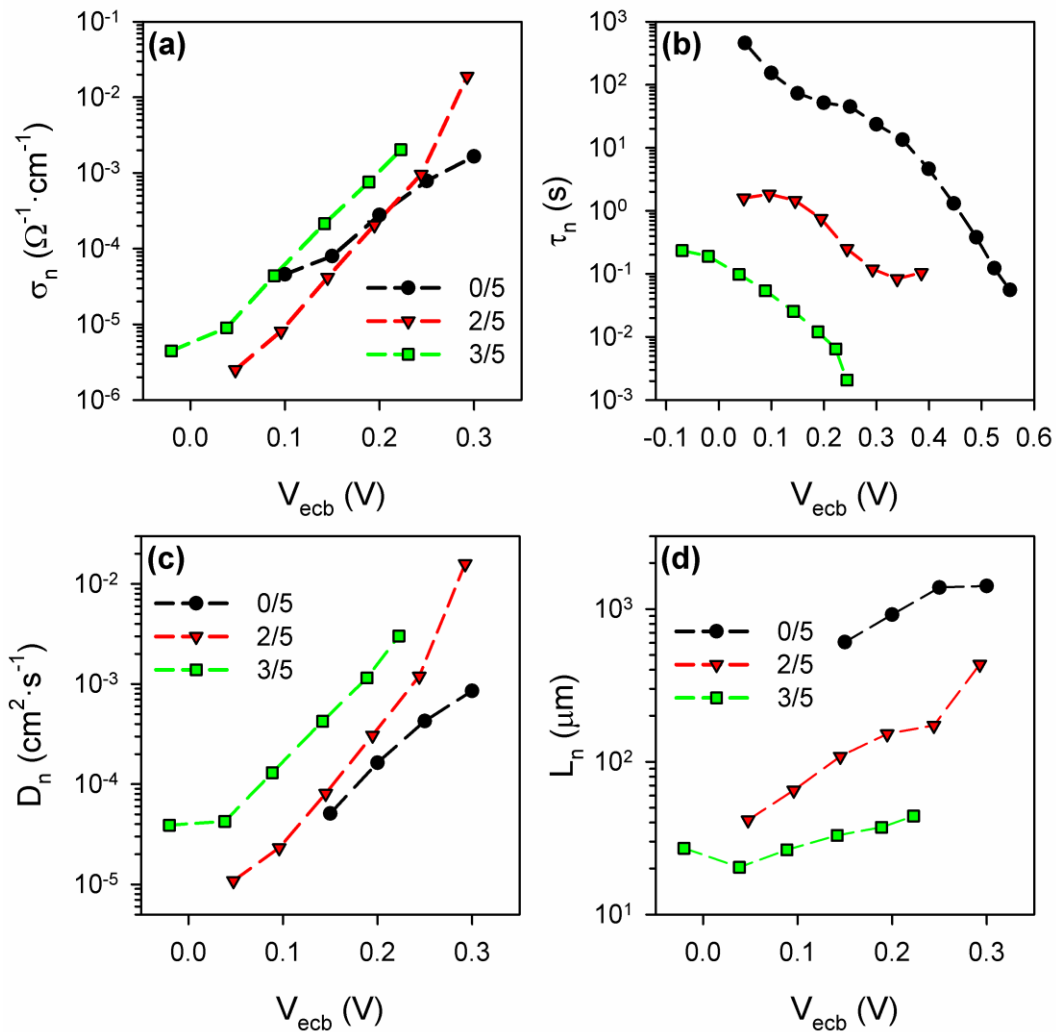


Fig. 5: (a) Electron conductivity in TiO₂, σ_n ; (b) electron lifetime, τ_n ; (c) electron diffusion coefficient, D_n , and (d) diffusion length L_n nanostructured TiO₂, for PbS/CdS/ZnS QDSC sensitized by SILAR using different number of PbS/CdS cycles as indicated in the legend and 2 SILAR cycles of ZnS, TiO₂ nanoparticles have been used for nanostructured electrode, polysulfide electrolyte and Cu₂O counter electrode.¹⁴ Reproduced with the permission of Journal of Physical Chemistry Letters.

The lifetime, τ_n , is the average time that excited electron "lives" before recombine. It can be calculated using the parameters obtained from impedance analysis as²⁹:

$$\tau_n = R_{rec} \cdot C_{\mu} \quad (3)$$

For the cases analyzed in Fig. 5(b) it can be observed that the lifetime decreases dramatically with the number of PbS SILAR cycles. This fact is indicative of an active role of PbS in the recombination process.

Diffusion coefficient of electrons in TiO₂, D_n , can also be obtained from IS characterization as:

$$D_n = L^2 / R_{tr} \cdot C_{\mu} \quad (4)$$

the tendency of D_n in Fig. 5(c) is the opposite that the observed for lifetime, increasing as the number of PbS SILAR cycles increases. But this effect is not enough to compensate the observed decrease in τ_n , from both parameters it can be extracted the diffusion length, L_n , that it is the distance traveled by an electron before recombining:

$$L_n = \sqrt{D_n \tau_n} \quad (5)$$

For a good cell performance L_n has to be higher than the thickness of the nanostructured electrode, L . In the case of the samples analyzed in Fig. 5(d) $L=14 \mu\text{m}$. Thus the cell with 3 SILAR cycles of PbS ($\eta=1.69 \%$) has a diffusion length that is only slightly higher than TiO₂ thickness. In this sense lower performance could be expected in comparison with the sample with 2 PbS SILAR layers ($\eta=2.21\%$). Obviously other effects have to be considered to determine the overall cause of the lower performance of the solar cell with 3 cycles of PbS, as light absorption. But in this case light absorption was higher for 3 cycles cell than for 2 cycles sample,¹⁴ concluding than the lower performance of 3 cycles cells is to the low lifetime. It is important to note that the definition of L_n given in eq. 5 is valid in the case of a linear recombination, that it is not the case of sensitized solar cells.³² In this broad context the square root of D_n times τ_n can be considered small perturbation diffusion length, and its interpretation is comparison with the electrode thickness is not straight forward and it is outside of the scope of this chapter. It is therefore recommended the discussion in terms of chemical capacitance and recombination resistance with an easier physical interpretation.

In summary, we have shown that impedance spectroscopy is a powerful tool to characterize quantum dot sensitized solar cells. For a proper characterization an equivalent circuit model with physical meaning have to be employed to fit the experimental data. From the fitting, an array of important parameters for solar cell performance can be obtained: series resistance, chemical capacitance, recombination resistance, counter electrode resistance, conductivity, lifetime, and diffusion coefficient. IS allows to decouple a complex system, the sensitized solar cells, in the different parts that constitute it, allowing a global characterization of the device.

References

1. Mora-Seró, I.; Garcia-Belmonte, G.; Boix, P. P.; Vázquez, M. A.; Bisquert, J., Impedance spectroscopy characterisation of highly efficient silicon solar cells under different light illumination intensities. *Energy & Environmental Science* 2009, 2, 678–686.
2. Mora-Seró, I.; Luo, Y.; Garcia-Belmonte, G.; Bisquert, J.; Muñoz, D.; Voz, C.; Puigdollers, J.; Alcubilla, R., Recombination rates in heterojunction silicon solar cells analyzed by impedance spectroscopy at forward bias and under illumination. *Solar Energy Materials and Solar Cells* 2008, 92, 505–509.
3. Proskuryakov, Y. Y.; Durose, K.; Al Turkestani, M. K.; Mora-Seró, I.; Garcia-Belmonte, G.; Fabregat-Santiago, F.; Bisquert, J.; Barrioz, V.; Lamb, D.; Irvine, S. J. C.; Jones, E. W., Impedance spectroscopy of thin-film CdTe/CdS solar cells under varied illumination. *Journal of Applied Physics* 2009, 106, 044507.
4. Bisquert, J., Theory of the Impedance of Electron Diffusion and Recombination in a Thin Layer. *The Journal of Physical Chemistry B* 2002, 106, 325–333.
5. Fabregat-Santiago, F.; Garcia-Belmonte, G.; Mora-Seró, I.; Bisquert, J., Characterization of nanostructured hybrid and organic solar cells by impedance spectroscopy. *Physical Chemistry Chemical Physics* 2011, 13, 9083–9118.
6. Wang, Q.; Ito, S.; Grätzel, M.; Fabregat-Santiago, F.; Mora-Seró, I.; Bisquert, J.; Bessho, T.; Imai, H., Characteristics of High Efficiency Dye-Sensitized Solar Cells. *Journal of Physical Chemistry C* 2006, 110, 25210–25221.
7. Rühle, S.; Shalom, M.; Zaban, A., Quantum-Dot-Sensitized Solar Cells. *Chemical Physics Chemistry* 2010, 11, 2290 – 2304.
8. Mora-Seró, I.; Bisquert, J., Breakthroughs in the Development of Semiconductor-Sensitized Solar Cells. *Journal of Physical Chemistry Letters* 2010, 1, 3046–3052.
9. Hodes, G., Comparison of Dye- and Semiconductor-Sensitized Porous Nanocrystalline Liquid Junction Solar Cells. *Journal of Physical Chemistry C* 2008, 112, 17778–17787.
10. Kamat, P. V., Quantum Dot Solar Cells. Semiconductor Nanocrystals as Light Harvesters. *Journal of Physical Chemistry C* 2008, 112, 18737–18753.
11. Kamat, P. V.; Tvrđy, K.; Baker, D. R.; Radich, J. G., Beyond Photovoltaics: Semiconductor Nanoarchitectures for Liquid-Junction Solar Cells. *Chemical Reviews* 2010, 110, 6664–6688.
12. Hetsch, F.; Xu, X.; Wang, H.; Kershaw, S. V.; Rogach, A. L., Semiconductor Nanocrystal Quantum Dots as Solar Cell Components and Photosensitizers: Material, Charge Transfer, and Separation Aspects of Some Device Topologies. *Journal of Physical Chemistry Letters* 2011, 2, 1879–1887.
13. Yang, Z.; Chen, C.-Y.; Roy, P.; Chang, H.-T., Quantum dot-sensitized solar cells incorporating nanomaterials. *Chemical Communications* 2011, 47, 9561–9571.
14. Braga, A.; Giménez, S.; Concina, I.; Vomiero, A.; Mora-Seró, I., Panchromatic sensitized solar cells based on metal sulfide quantum dots/panchromatic sensitized solar cells based on metal sulfide quantum dots. *Journal of Physical Chemistry Letters* 2011, 2, 454–460.
15. González-Pedro, V.; Xu, X.; Mora-Seró, I.; Bisquert, J., Modeling High-Efficiency Quantum Dot Sensitized Solar Cells. *ACS Nano* 2010, 4, 5783–5790.
16. Mora-Seró, I.; Giménez, S.; Fabregat-Santiago, F.; Gómez, R.; Shen, Q.; Toyoda, T.; Bisquert, J., Recombination in Quantum Dot Sensitized Solar Cells. *Accounts of Chemical Research* 2009, 42, 1848–1857.

17. Hossain, M. A.; Jennings, J. R.; Koh, Z. Y.; Wang, Q., Carrier Generation and Collection in CdS/CdSe-Sensitized SnO₂ Solar Cells Exhibiting Unprecedented Photocurrent Densities. *ACS Nano* 2011, 5, 3172–3181.
18. Barea, E. M.; Shalom, M.; Giménez, S.; Hod, I.; Mora-Seró, I.; Zaban, A.; Bisquert, J., Design of Injection and Recombination in Quantum Dot Sensitized Solar Cells. *Journal of the American Chemical Society* 2010, 132, 6834–6839.
19. Fabregat-Santiago, F.; Bisquert, J.; Garcia-Belmonte, G.; Boschloo, G.; Hagfeldt, A., Influence of electrolyte in transport and recombination in dye-sensitized solar cells studied by impedance spectroscopy. *Solar Energy Materials and Solar Cells* 2005, 87, 117-131.
20. Acharya, K. P.; Khon, E.; O'Conner, T.; Nemitz, I.; Klinkova, A.; Khnayzer, R. S.; Anzenbacher, P.; Zamkov, M., Heteroepitaxial Growth of Colloidal Nanocrystals onto Substrate Films via Hot-Injection Routes. *ACS Nano* 2011, 5, 4953-4964.
21. Boix, P. P.; Larramona, G.; Jacob, A.; Delatouche, B.; Mora-Seró, I.; Bisquert, J., Hole Transport and Recombination in All-Solid Sb₂S₃-Sensitized TiO₂ Solar Cells Using CuSCN As Hole Transporter. *Journal of Physical Chemistry C* 2012, 116, 1579–1587.
22. Boix, P. P.; Lee, Y. H.; Fabregat-Santiago, F.; Im, S. H.; Mora-Seró, I.; Bisquert, J.; Seok, S. I., From Flat to Nanostructured Photovoltaics: Balance between Thickness of the Absorber and Charge Screening in Sensitized Solar Cells. *ACS Nano* 2012, 6, 873–880.
23. Mora-Seró, I.; Giménez, S.; Fabregat-Santiago, F.; Azaceta, E.; Tena-Zaera, R.; Bisquert, J., Modeling and characterization of extremely thin absorber (eta) solar cells based on ZnO nanowires. *Physical Chemistry Chemical Physics* 2011, 13, 7162–7169.
24. Fabregat-Santiago, F.; Bisquert, J.; Cevey, L.; Chen, P.; Wang, M.; Zakeeruddin, S. M.; Grätzel, M., Electron Transport and Recombination in Solid-State Dye Solar Cell with Spiro-OMeTAD as Hole Conductor. *Journal of American Chemical Society* 2009, 131, 558-562.
25. Sudhagar, P.; González-Pedro, V.; Mora-Seró, I.; Fabregat-Santiago, F.; Bisquert, J.; Kang, Y. S., Interfacial Engineering of Quantum Dot-Sensitized TiO₂ Fibrous Electrodes for Futuristic Photoanodes in Photovoltaic Applications. *Journal of Materials Chemistry* 2012, DOI:10.1039/C2JM31599H.
26. Lee, H. J.; Wang, M.; Chen, P.; Gamelin, D. R.; Zakeeruddin, S. M.; Grätzel, M.; Nazeeruddin, M. K., Efficient CdSe Quantum Dot-Sensitized Solar Cells Prepared by an Improved Successive Ionic Layer Adsorption and Reaction Process. *Nano Letters* 2009, 9, 4221-4227.
27. Lee, H. J.; Leventis, H. C.; Moon, S.-J.; Chen, P.; Ito, S.; Haque, S. A.; Torres, T.; Nüesch, F.; Geiger, T.; Zakeeruddin, S. M.; Grätzel, M.; Nazeeruddin, M. K., PbS and CdS Quantum Dot-Sensitized Solid-State Solar Cells: “Old Concepts, New Results”. *Advanced Functional Materials* 2009, 19, 2735–2742.
28. Sze, S. M., *Physics of Semiconductor Devices*. 2nd ed.; John Wiley and Sons: New York, 1981.
29. Bisquert, J.; Fabregat-Santiago, F.; Mora-Seró, I.; Garcia-Belmonte, G.; Giménez, S., Electron Lifetime in Dye-Sensitized Solar Cells: Theory and Interpretation of Measurements. *Journal of Physical Chemistry C* 2009, 113, 17278–17290.
30. Barea, E. M.; Ortiz, J.; Pay, F. J.; Fernández-Lázaro, F.; Fabregat-Santiago, F.; Sastre-Santos, A.; Bisquert, J., Energetic Factors Governing Injection, Regeneration and Recombination in Dye Solar Cells with Phthalocyanine Sensitizers. *Energy & Environmental Science* 2010, 3, 1985–1994.

31. Bisquert, J., Chemical capacitance of nanostructured semiconductors: its origin and significance for nanocomposite solar cells. *Physical Chemistry Chemical Physics* 2003, 5, 5360-5364.
32. Bisquert, J.; Mora-Seró, I., Simulation of Steady-State Characteristics of Dye-Sensitized Solar Cells and the Interpretation of the Diffusion Length. *Journal of Physical Chemistry Letters* 2010, 1, 450–456.